Two-dimensional P-T-t modelling and the dynamics of extension and compression in the Betic Zone (SE Spain)

van Wees, J.D.; de Jong, K.; Cloetingh, S.A.P.L.

published in
Tectonophysics
1992

document version
Publisher's PDF, also known as Version of record

Tectonophysics, 203 (1992) 305–324
Elsevier Science Publishers B.V., Amsterdam

Two-dimensional *P–T–t* modelling and the dynamics of extension and inversion in the Betic Zone (SE Spain)

J.D. van Wees, K. de Jong and S. Cloetingh

Institute of Earth Sciences, Vrije Universiteit, De Boelelaan 1085, 1081 HV Amsterdam, The Netherlands

(Received December 14, 1990; revised version accepted April 15, 1991)

ABSTRACT

Van Wees, J.D., De Jong, K. and Cloetingh, S., 1992. Two-dimensional *P–T–t* modelling and the dynamics of extension and inversion in the Betic Zone (SE Spain). In: E. Banda and P. Santanach (Editors), Geology and Geophysics of the Valencia Trough, Western Mediterranean. *Tectonophysics*, 203: 305–324.

The Internal Zone of the Betic Cordilleras offers a unique opportunity to study the dynamics of lithospheric processes at mid crustal levels, which controlled the formation and evolution of the southeastern margin of Iberia. In this paper we present the result of two-dimensional numerical modelling of *P–T–t* paths related to latest Oligocene and Early Miocene extension and inversion in the Betic Zone. The ages of *P–T–t* loops are constrained by an extensive data set of geothermo-barometric and geochronological data, including $^{40}Ar/^{39}Ar$ laser probe data. We investigate the thermo-mechanical evolution of the Betic Zone using numerical models for simple shear, pure shear and combined shear. The Wernicke simple shear model fails to explain the observed temperatures in excess of 500°C and is not consistent with the occurrence of intrusions of ultramafic rocks in the western Betics. However, the delaminated simple shear model with low-angle faults located only at lower crustal levels, is found to be consistent with the *P–T–t* data.

After a heating phase, associated with a finite extension of 80 km, rapid cooling occurred reflecting inversion of the extensional structure by NW–SE to N–S directed compression. Palaeo-rheological models for the latest Oligocene–Early Miocene times demonstrate the important role of the detachments produced during crustal extension for the dynamics of the subsequent inversion phase. The modelling strongly suggest that inversion locked after 60 km of finite convergence. After locking of the inversion, overthrusting in a northward direction occurred, which is compensated by pure shear deformation in the lower crust in the southeastern part of the Betic Zone.

Introduction

The eastern margin of Iberia forms the southern termination of the West European Rift system (Fig. 1). The main basins in the Iberian branch of this system, the Valencia trough and the Alborán basin were formed in a late Oligocene and younger extensional tectonic regime (Vegas and Banda, 1982; Banda et al. 1983; Rehault et al., 1984; Fontboté et al., 1990). Seismic data show that the crustal thickness of the Iberian Peninsula diminishes towards these offshore basins (Banda and Ansorge, 1980; Banda et al., 1983; Zeyen et al., 1985). This feature is also clearly expressed by the pattern of Bouguer anomalies (Van den Bosch, 1974; Casas and Carbó, 1990). The magnetic characteristics of both the Alborán basin and the Valencia trough suggest that these are underlain by strongly attenuated continental crust (Galdeano and Rossignol, 1977). The presence of relatively large masses of ultramafic rocks in the westernmost Betics and northern Morocco (Kornprobst, 1969; Loomis, 1975; Westerhof, 1977) indicate that extensional tectonics also involved the subcrustal lithosphere in the area.

Both the Valencia trough and the Alboran Basin (Fig. 1) are the site of concentrated Burdigalian and younger volcanism of calc-alkaline and

Correspondence to: J.D. van Wees, Vrije Universiteit, Institute for Earth Sciences, De Boelelaan 1085, 1081 HV Amsterdam, The Netherlands.

alkaline affinity (Ferrara et al., 1973; Bellon and Brousse, 1977; Martí et al., 1990). Furthermore, the Valencia trough is characterized by an elevated heat flow, which continues southeastwards into the Betic Cordilleras (Albert-Bertrán, 1979; Maillard et al., 1990). The Betic Cordilleras experienced an important phase of reheating (Bakker et al., 1989; De Jong, 1990) related to extension tectonics.

The Alborán Basin is nearly completely surrounded by metamorphic rocks of the Betic-Rif orogen, whereas the Valencia trough formed at the location of a Mesozoic and Tertiary basin. Similarity in timing and nature of tectonic events in both rifted basins indicates that they reflect the same geodynamic process, now exposed at different erosional levels. The Internal Zone of the Betic Cordilleras offers the possibility of studying the dynamics of the extensional and inversion tectonics at mid-crustal and deeper levels. Furthermore, a high quality P–T–t database (De Jong, 1991) for the area has enabled investigation of the spatial and temporal variation in tectonic processes. Previous work was focused on

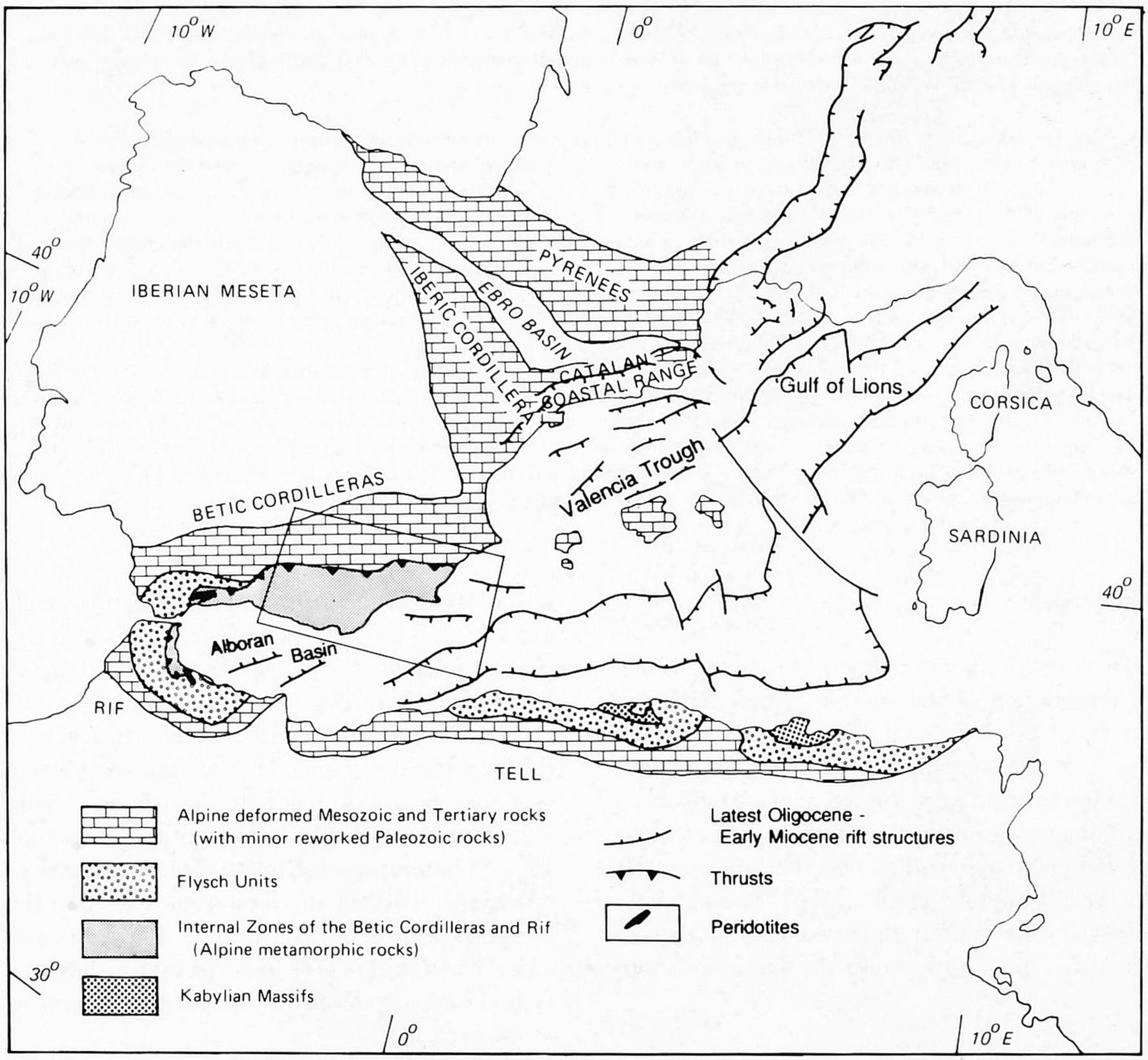

Fig. 1. Sketch map of the westernmost Mediterranean area (modified after Ricou et al., 1986), showing the major Alpine structural provinces. The location of the eastern Betic Cordilleras of southern Spain is indicated by the inset. Rift structures modified after Rehault et al., 1984.

the tectono-metamorphic evolution of the Betic Zone, based on *P–T–t* data (Bakker et al., 1989; De Jong, 1990, 1991) and geochronological data (De Jong et al., 1992). Here we present the results of a two-dimensional *P–T–t* modelling study of the dynamics of extension and inversion in the eastern Betic Cordilleras, constrained by these data sets.

Tectonic setting

The Betic Cordilleras can be subdivided in the Internal Zone (or Betic Zone) and the External Zone (Figs. 1 and 2). The Internal Zone in the eastern Betics consists of a stack of four tectonic complexes, from top to bottom (Fig. 2): the Maláguide complex, Alpujárride complex, Mulhacén complex, and Veleta complex. These complexes are separated by subhorizontal, low-angle faults or mylonite zones. A fifth complex, the Almágride complex, which has a stratigraphic resemblance to tectonic units in the External Zone (Simon, 1987), falls beyond the scope of the present study. The lowest three complexes experienced plurifacial metamorphism during the polyphase Alpine tectonics (Gómez-Pugnaire and Fernández-Soler, 1987; Bakker et al., 1989; De Jong, 1990, 1991), whereas the Maláguide complex consists of unmetamorphozed or very low-grade metamorphic rocks (Durand-Delga, 1968; Egeler and Simon, 1969). The External Zone consists of deformed sediments originally deposited on the Mesozoic Betic rifted margin. A discussion of the tectonic subsidence of these sequences is given by Peper and Cloetingh (1992-this volume).

In the present study, we focus on the modelling of the thermo-tectonic evolution of the Mulhacén complex and Alpujárride complex in the Internal Zone. The *P–T–t* path of the Mulhacén complex (Tables 1, 2; Fig. 3) displays the main elements of the lithospheric scale tectonics, which were involved in the evolution of the Betic Cordilleras. Alpine HP–LT metamorphism resulted from subduction and was followed by isobaric heating as a consequence of relaxation of the depressed isotherms. Later decompression and cooling occurred, at the end of which a new steady-state thermal and lithospheric configuration was established. During the early stages of decompression two penetrative ductile deformation phases occurred (D1 and D2, Fig. 3), which document significant westward thrusting of the Alpujárride complex on top of the Mulhacén complex. Extensive reheating was the result of latest Oligocene–Early Miocene extensional tec-

TABLE 1

P–T–t data of the Mulhacén complex in the eastern Sierra de Los Filabres (after Bakker et al., 1989; De Jong, 1991; De Jong et al., 1992)

P–T–t	*P* (GPa)	*T* (°C)	*t* (Ma)	Description
Ar2		360 ± 50	21–22	Modelled $^{40}Ar/^{39}Ar$ phengite cooling ages, inferred from $^{40}Ar/^{39}Ar$ age plateaus
D4	0.25–0.45	450–525		Peak heating
D3	0.3 –0.4	350–425	ca. 25	Low-grade metamorphism. Starting heating + partial thermal resetting of $^{40}Ar/^{39}Ar$ cooling ages, inferred from phengite single grain
Ar1		360 ± 50	30–31	Oldest $^{40}Ar/^{39}Ar$ cooling ages in core of phengite single grain
C	0.4 –0.55	400–500		Cooling trajectory
Rb1		500 ± 50	65 ± 10	$^{87}Rb/^{86}Sr$ phengite cooling age
D2	0.7 –1.0	525–575		Medium-grade metamorphism, synkinematic decompression, main tectono-metamorphic phase
D1	0.9 –1.1	475–525		Synkinematic eclogitization/ glaucophane schist facies
B	1.0 –1.1	375–425		Static eclogitization
A	1.0 –1.1	300		Incipient eclogitization

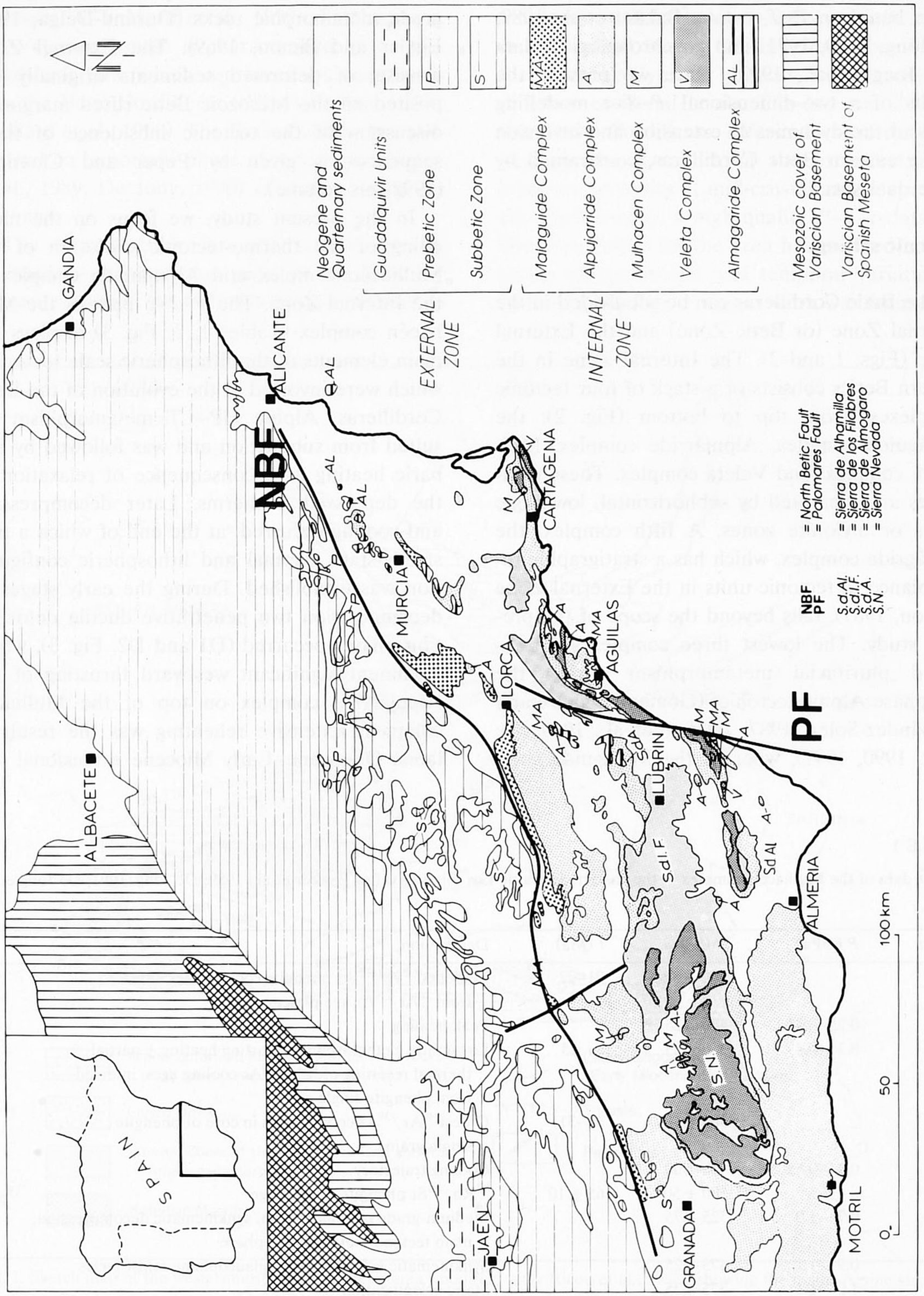

Fig. 2. Tectonic sketch map of the eastern Betic Cordilleras showing the distribution of major tectonic complexes (after Bakker et al., 1989).

tonics, reflected by the penetrative ductile deformation phase, D3. The extension was followed by N–S directed compression, which resulted in the ductile deformation phase, D4. At the end of D4 the Alpujárride complex was transported northward relative to the Mulhacén complex, along

TABLE 2

Tectonic model for the Mulhacen Complex $P-T-t$ evolution (after Bakker et al, 1989; De Jong, 1990, 1991)

		t (Ma)	Phase
		21–19	Early Miocene compression
Ar2	21		
		23–21	Early Miocene compression
D4			
		28–23	latest Oligocene extension
D3			
		30–28	latest Oligocene plate reorganisation
Ar1	30		
C			
		80–30	relaxation
Rb1	65		
D2			Cretaceous
D1			
		110–80	subduction + collision
B			
A			

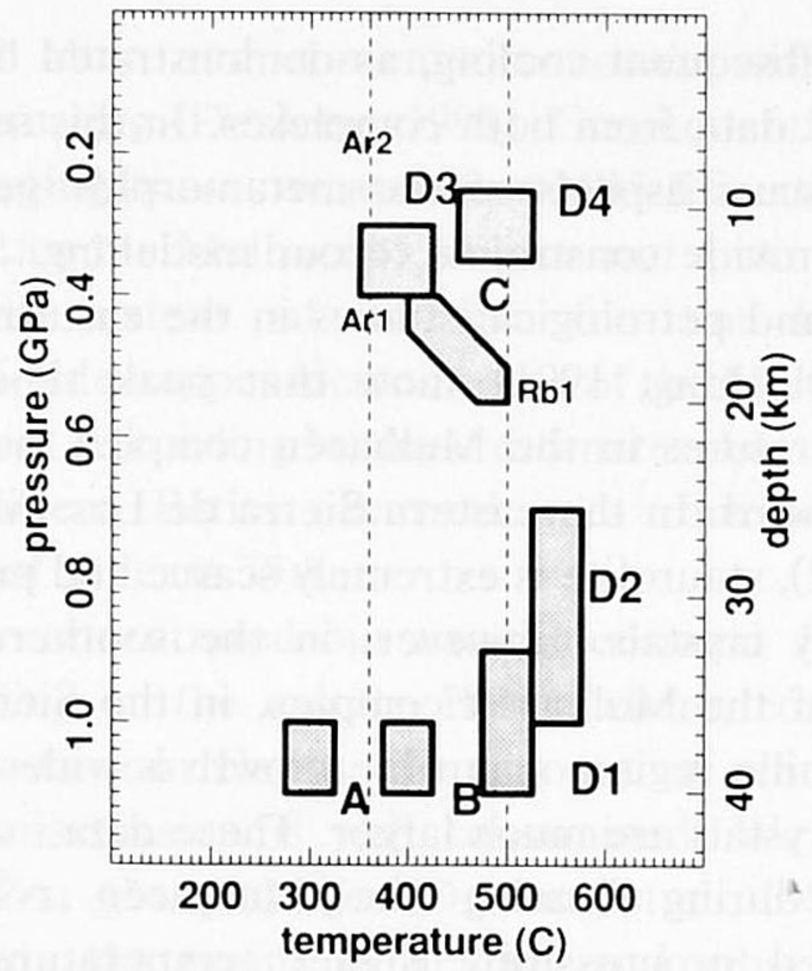

Fig. 3. $P-T-t$ data of the Mulhacén complex in the eastern Sierra de Los Filabres (after Bakker et al., 1989; De Jong, 1991; De Jong et al., 1992). Boxes A, B, C, D1, D2, D3 and D4 correspond to metamorphic phase constraints. D1, D2, D3 and D4 indicate major deformation phases. Ar1 and Ar2 reflect phengite cooling ages obtained from $^{40}Ar/^{39}Ar$ dating. Rb1 reflects phengite cooling ages, obtained from $^{87}Rb/^{86}Sr$ dating. For ages see Table 1.

mylonite zones which (Behrmann and Platt, 1982; De Jong, 1991). Subsequently, the ductile structures were influenced by brittle–ductile imbrications and normal faulting.

In the present paper we focus on the numerical modelling of the latest Oligocene–Early Miocene reheating and cooling of the Mulhacén complex and Alpujárride complex in the Betic Zone. The present outcrops of tectonic complexes in the Internal Zone are dominated by strike-slip features and normal faulting (see Peper and Cloetingh, 1992-this volume, for an extensive discussion), which postdates the latest Oligocene–Early Miocene evolution. A detailed treatment of late stage, E–W gradients in the distribution of metamorphism and tectonic units, however, falls beyond the scope of the present paper.

Constraints provided by $P-T-t$ data and structural interpretation

Both the Mulhacén and Alpujárride complexes document significant extension-related reheating

and subsequent cooling, as demonstrated by the *P–T–t* data from both complexes. In this section we discuss aspects of the metamorphic geology that provide constraints to our modelling. Structural and petrological studies in the eastern Betics (De Jong, 1991) show that peak reheating temperatures in the Mulhacén complex increase southward. In the eastern Sierra de Los Filabres (Fig. 2), staurolite is extremely scarce and present as tiny crystals. However, in the southernmost part of the Mulhacén complex, in the Sierra de Alhamilla region, staurolite growth is widespread and crystals are much larger. These data indicate that, during heating the Mulhacén complex reached progressively higher temperatures towards the southeast.

In the Alpujárride complex a distinction exists between higher and lower nappes (Simon et al., 1976). In this sequence, the lower Alpujárride nappes experienced the same or less reheating than the Mulhacén complex, as is indicated by metamorphic data (Bakker et al., 1989). However, widespread occurrence of staurolite in higher Alpujárride nappes, demonstrates that this zone experienced a more intense heating phase than the Mulhacén complex and the lower Alpujárride nappes. At present, the higher Alpujárride complex regionally overlies both the Mulhacén complex and the lower Alpujárride nappes as a result of late D4 overthrusting. This implies that the overthrusting contact was formed after heating. The northward sense of shear in mylonites in the eastern Betic Zone indicate that the higher Alpujárride nappes were situated more to the south than the Mulhacén complex and lower Alpujárride nappes during heating. In part, the more southern position of the higher Alpujárride nappes can be explained by an extensional process which involved translation of the Alpujárride complex urth respect to the Mulhacén complex along a south-dipping detachment zone (Fig. 4A). The presence of this zone is supported by field mapping, which revealed a complete southward excision of the Mulhacén complex from the Sierra de Los Filabres to the Sierra de Alhamilla (De Jong, 1991, Fig. 4).

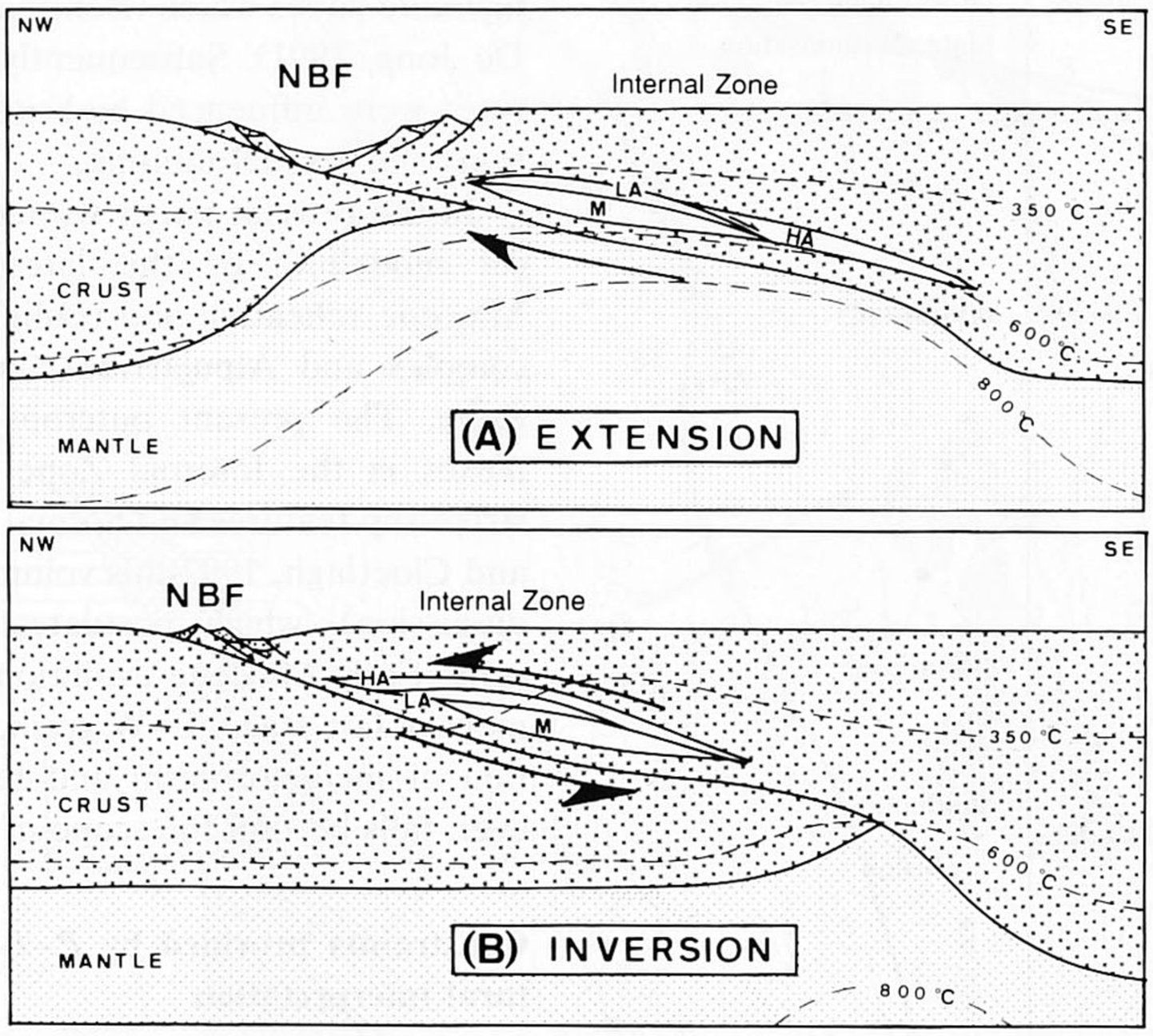

Fig. 4. Schematic N–S paleo-cross sections through the eastern Betics for (A) latest Oligocene–Early Miocene extension and (B) subsequent inversion. *HA* = higher Alpujárride nappes; *LA* = lower Alpujárride nappes; *M* = Mulhacén complex; *NBF* = North Betic fault.

Heating in the eastern Betics occurs simultaneously with advection of ultramafic rocks to crustal levels in the westernmost Betics (Bakker et al., 1989). Subsequent ductile emplacement of ultramafic rocks on top of Alpujárride nappes is related to a compressional phase (Tubía and Cuevas, 1986). The position of ultramafic rocks, on top of upper crustal rocks of the Alpujárride complex, indicates that the present configuration is the result of thrusting (Westerhof, 1977; Lundeen, 1978) and inversion of the extensional structure. The interpretation in terms of thrusting is in agreement with seismic refraction interpretations (Barranco et al., 1990). Thrust emplacement resulted in the formation of leucogranites in the country rock as a result of anatexis at the contact, which yielded a $^{87}Rb/^{86}Sr$ mineral isochron cooling age of 22 ± 4 Ma (Priem et al., 1979). The metamorphic grade of the Alpujárride complex increases towards the ultramafic rocks and reheating temperatures in the Alpujárride complex associated with the ultramafic rocks are of the order of 700–750°C (Loomis, 1975; Westerhof, 1977; Torres-Roldán, 1981).

The position of ultramafic rocks and high grade metamorphic contact aureoles in the westernmost Betics, points to a similar scenario in the eastern Betics, which supports widespread heating in the Alpujárride and Mulhacén complexes by advection of mantle rocks to crustal levels. Furthermore, the, generally higher, Alpujárride nappes in the eastern Betics exhibit high-grade metamorphism in the basal parts, with sillimanite or staurolite growth, which does not occur in the upper levels (Triassic series). This high vertical gradient in metamorphism points to a highly elevated vertical heat flow during extension, or to thinning of the metamorphic column following the heating phase.

The regional distribution of heated parts of the Mulhacén and Alpujárride complexes in the eastern Betics (Fig. 2), demonstrates that the present outcrop of the heating zone has length of at least 300 km in a NE–SW direction and a maximum width of 80 km. The higher Alpujárride nappes have been thrust over the Mulhacén complex and the lower Alpujárride nappes, after the heating phase, and considerable extension occurred after and contemporaneously with this overthrusting (De Jong, 1991). Consequently, for the heating phase, we assume a NW–SE extent of 50 km for the Mulhacén complex and a minimum NW–SE extent of 25 km for the higher Alpujárride nappes located south of the Mulhacén complex. According to these estimates, heating in the eastern Betics occurred in a zone with a width of at least 75 km.

We concentrated our two-dimensional *P–T–t* modelling on the eastern Betics where, contrary to the western Betics, the amount of reheating due to extension is well constrained. We used $^{40}Ar/^{39}Ar$ phengite ages (De Jong et al., 1992) to constrain the timing of heating and subsequent cooling. The phengite ages are interpreted as cooling ages, using the closure temperature of muscovite (360 ± 50°C) according to Purdy and Jäger (1976). $^{40}Ar/^{39}Ar$ laser probe dating in a 3 mm wide single crystal resulted in ages of 31–30 Ma in the core, and progressively younger ages, to about 25 Ma, in the rim (De Jong et al., 1992). For the present modelling the 30 Ma age (Ar1 in Tables 1 and 2; Fig. 3) is taken as the time at which the Mulhacén complex reached a new thermal steady state. The progressively younger ages towards the rim indicate thermal resetting, which is related to heating. As a time constraint for cooling after heating, a timing of 21 Ma is adopted (Ar2 in Tables 1 and 2; Fig. 3), which is based on modelling of $^{40}Ar/^{39}Ar$ age spectra (De Jong et al., 1992).

Tectonically, we interpret the heating in terms of a model of simple shear extension (Figs. 5,6) (Wernicke, 1981; Lister et al., 1986; Kusznir et al., 1987) along a low-angle southeast–south-dipping master fault. In this model, the Mulhacén and Alpujárride complexes are located in the hanging wall and heated by advection from the footwall. The trend of possible simple shear detachments in the extensional setting is parallel to the orientation of master faults in the Betics, like the North Betic fault, and continuous trends in Bouguer anomalies (Van den Bosch, 1974; Casas and Carbó, 1990) and crustal thickness (Banda, 1988). Temperatures in the Mulhacén complex were probably not raised prior to 25 Ma, as indicated by resetting ages. Consequently, we

consider this age as a minimum for the onset of the simple shear extension, while we assume a timing of 28 Ma for the onset of extension.

During inversion of the extensional structure, the Mulhacén complex was rapidly cooled from peak temperature conditions (500°C) to a temperature of 360°C at 21 Ma (Ar2 in Tables 1 and 2; Fig. 3). The onset of inversion, therefore, must be prior to 21 Ma and an estimate of 23 Ma for this timing is adopted here. It seems that no significant erosional exhumation of the Mulhacén complex occurred during cooling, as Neogene sedimentary basins surrounding the eastern Sierra de Los Filabres do not record substantial amounts of coarse clastic sediment infill in Aquitanian and Burdigalian times (Völk and Rondeel, 1964). The southern part of the Mulhacén complex shows an inverted metamorphic gradient, which is probably due to subsequent thrusting of the upper parts of the Alpujárride complex (De Jong, 1991). This

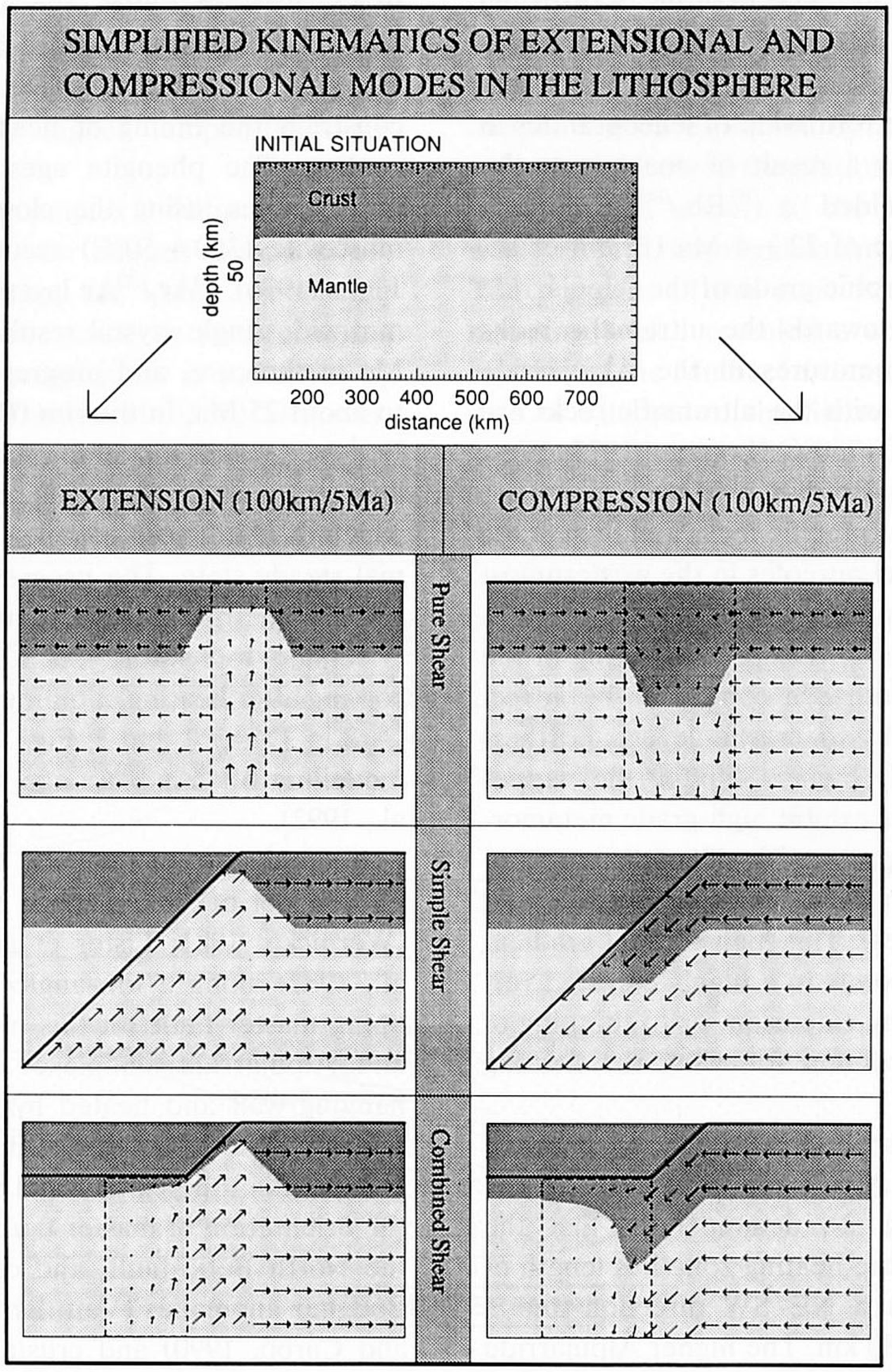

Fig. 5. Simplified kinematics of extensional and compressional modes in the lithosphere for models of pure shear, simple shear and combined shear (after Buck et al., 1988; Kusznir et al., 1987). Velocity fields for deformation are indicated by arrows. Dashed boxes indicate areas of pure shear deformation.

feature indicates that during inversion, the higher Alpujárride nappes did not undergo significant cooling and were mainly cooled at the overthrusting stage, which corresponds to slightly younger cooling ages of 19 Ma for higher Alpujárride nappes (Monié et al., 1991). The overthrusting in the upper crust is assumed to be accompanied by lower crustal pure shear thickening.

Numerical modelling of the *P–T–t* evolution

Thermal modelling

For the numerical modelling of the *P–T–t* evolution a two-dimensional explicit 3-step Runge-Kutta finite difference approach was used (Verwer, 1977). In the finite difference approach,

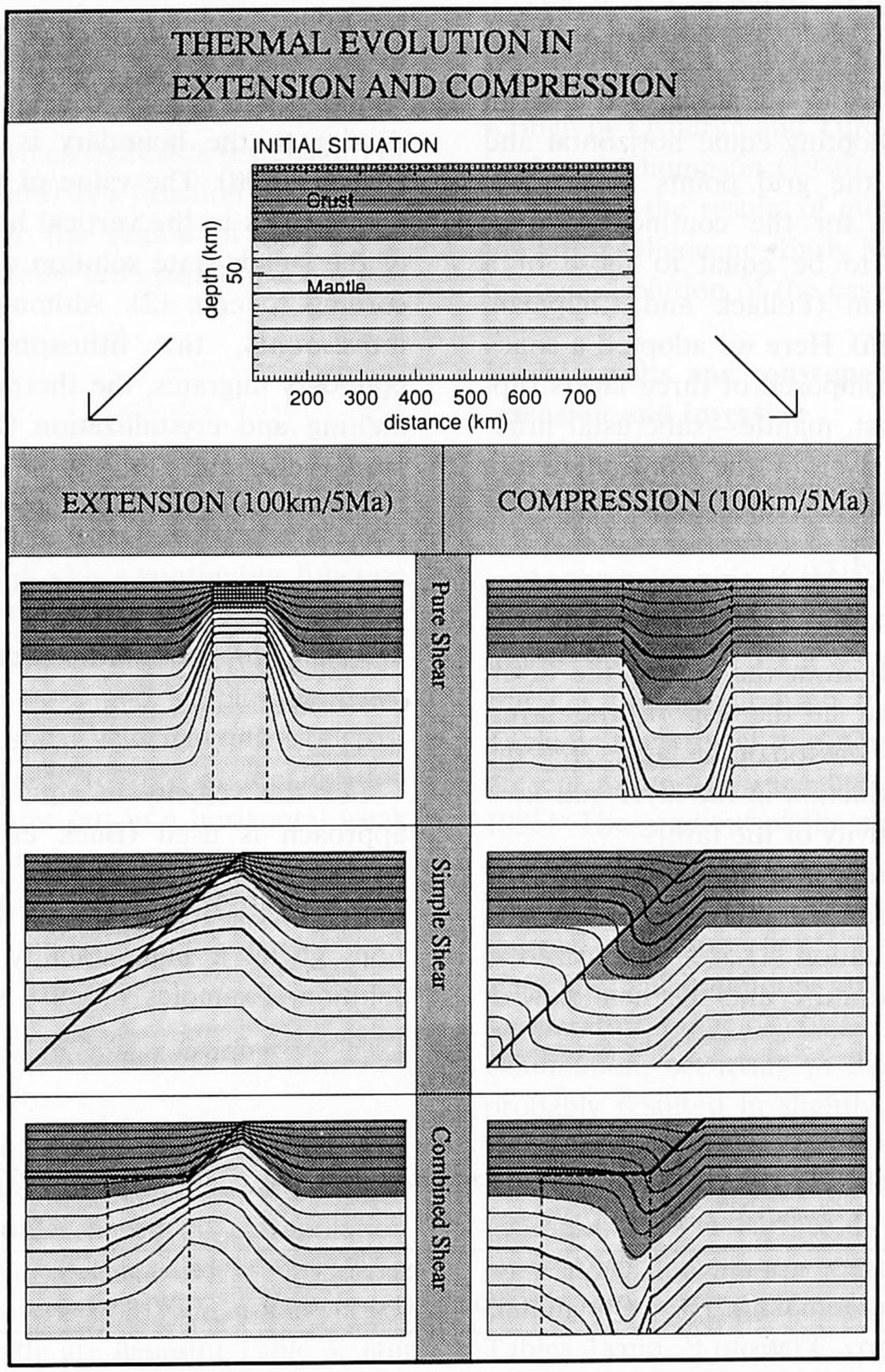

Fig. 6. Thermal evolution in extension and compression, according to the kinematics, outlined in Fig. 5. Solid lines = temperature distribution (contoured in intervals of 100°C); dashed lines indicate areas of pure shear deformation.

temperatures in a two-dimensional grid were traced in time by integration of the heat conduction equation:

$$\frac{\partial T}{\partial t} = \frac{1}{\rho c_p}\left[\nabla \cdot (k\ \nabla T) + A\right] - \vec{v} \cdot \nabla T \qquad (1)$$

where: T = temperature, ρ = density; c_p = specific heat; k = thermal conductivity, A = radiogenic heat production and $\vec{v}$ = velocity vector.

In the numerical analysis, grid dimensions, initial temperatures, material properties, boundary conditions and velocity field had to be determined. A rectangular grid was used, which covered an area with a width of 750 km and a depth range of 250 km, adopting equal horizontal and vertical spacing of the grid points of 2.5 km. Initial temperatures for the continental lithosphere were taken to be equal to those of a steady-state geotherm (Pollack and Chapman, 1977; Chapman, 1986). Here we adopted a continental lithosphere composed of three layers (upper crust, lower crust, mantle—subcrustal lithosphere). For each layer of the lithosphere the temperature profile is described by:

$$T(z) = T_1 + \frac{Q_1 z}{k_1} - \frac{A_1 z^2}{2k_1} \qquad (2)$$

where z = the depth from the top of the layer; T_1 = the temperature at the top of the layer, Q_1 = the heat flow at the top of the layer; A_1 = the radiogenic heat production in the layer and k_1 = the thermal conductivity of the layer.

Material parameters used for the steady state geotherm of the stratified lithosphere, eqn. (2), and for the heat equation (1) are summarized in Table 3. The temperature and the heat flow at the top of the first layer correspond to a surface temperature ($T_s = 0$°C) and surface heat flow, Q_s, respectively. The transition from lithosphere to asthenosphere corresponds to $T = T_m$ (1325°C), where T_m = the melting temperature for ultramafic rocks. A constant temperature ($T = T_m$) is adopted for the asthenosphere. Following Pollack and Chapman (1977), we assume that the radiogenic heat production rate within the upper crust accounts for 40% of the surface heat flow.

During time integration, $\partial T/\partial x = 0$ at the left hand side and right hand side of the model. At the upper boundary temperatures are kept fixed to T_s, while at the asthenosphere–lithosphere boundary ($T = T_m$), a constant heat flow perpendicular to the boundary is adopted (Van den Beukel, 1990). The value of this basal heat flow corresponds to the vertical heat flow at the base of the steady-state solution of the geotherm, according to eqn. (2). Although, due to tectonic movements, the lithosphere–asthenosphere boundary migrates, the thermal effects of partial melting and crystallization (latent heat) associated with the migration of the boundary (Stephenson, 1989) are ignored in the present study.

Modelling of pure shear, simple shear and combined shear

For the velocity in eqn. (1), a velocity field approach is used (Buck et al., 1988). In our modelling, the velocity field associated to a tectonic process remains fixed during time integration, giving a high stability for the numerical solution. Examples of pure shear, simple shear

TABLE 3

Material parameters used in thermal modelling. (Thermal parameters after Pollack and Chapman, 1977; Chapman, 1986; Rock anologues after Carter and Tsenn, 1987)

Layer	Thickness (km)	Density (kg m^{-3})	Conductivity (W m^{-1} °C^{-1})	Specific heat (J kg^{-1} °C^{-1})	Heat production (μW m^{-3})	Rheology (rock analogue)
Upper crust	16	2800	2.6	1050	depends	quartzite (dry)
Lower crust	16	2800	2.6	1050	0.5	diorite (wet)
Mantle		3300	3.1	1050	0.0	dunite (wet)

and combined shear mechanisms, their velocity fields and thermal evolutions are given in Figs. 5 and 6.

Simple shear tectonics are simulated by two blocks separated by a fault, which move with different constant horizontal velocities. The velocities in each block satisfy the equation:

$$|\vec{v}|\cos\alpha = \text{constant} \qquad (3)$$

where $|\vec{v}|$ = the magnitude of the velocity vector (parallel to the fault plane) and α = the dip of the fault. Vertical motions arise from the dip of the fault, while bending of layers at hinge lines is accommodated by vertical shear.

We describe pure shear tectonics in terms of a horizontal velocity, which increases (extension) or decreases (compression) as a function of the horizontal coordinate in the region of the model undergoing deformation. We assume incompressible flow:

$$\frac{\partial v_x}{\partial x} = -\frac{\partial v_z}{\partial z} = f(x) \qquad (4)$$

If particles move through the velocity field based on a continuous function $f(x) = \partial v_x/\partial x$, the finite stretching $\beta(x)$ is a continuous function provided that $\partial^2 v_x/\partial x^2 = 0\,|_{v_x=0}$

We modelled combined shear tectonics by a combination of the pure and simple shear approach. The simple shear velocity contrast across the fault, Δv, decreases to zero at the location where the fault flattens out in a horizontal weak layer (lower crust). In the area of decreasing Δ_v, pure shear deformation occurs according to eqn. (4).

Rheological modelling and shear heating

The distribution of temperatures and materials enables the calculation of two-dimensional lithospheric strength profiles based on extrapolation of rock mechanics data (Carter and Tsenn, 1987). Rheological parameters used for upper crust, lower crust and mantle are listed in Table 3.

In simple shear tectonics, effects of heat dissipation are represented (Van den Beukel and Wortel, 1987; Molnar and England, 1990; Van den Beukel, 1990) by:

$$Q_f = \tau\,\Delta v \qquad (5)$$

where Q_f = heat dissipation rate per unit length along the fault; τ = shear stress on the fault and Δv = velocity contrast across the fault. Heat dissipation associated with pure shear deformation is ignored.

Construction of P–T–t paths

The *P–T–t* evolution of individual points was traced by tracking their burial depths and temperatures through time, similar to methods described by Oxburgh and Turcotte (1974) and England and Thompson (1986). In the next section, we present the results of numerical modelling of the latest Oligocene–Early Miocene phase of the tectonic evolution of the eastern Betics.

Model results and consequences for lithospheric extension and inversion

Initial lithospheric configuration

At the beginning of the tectonic evolution discussed here (28 Ma), the thermal situation is represented by the steady-state solution given in eqn. (2), adopting lithosphere parameters given in Table 3. The crustal thickness corresponds to the present value for the Iberian Meseta (Banda, 1988). The gradient of the steady-state geotherm is constrained by the *P–T–t* trajectory in box C (Fig. 3, Tables 1 and 2), in which near steady-state thermal conditions have been reached. Steady-state thermal conditions are chosen in the low temperature range of box C. This is because slow exhumation, occurring in this *P–T–t* trajectory, probably resulted in slightly higher temperature values than those corresponding to the steady-state geotherm. These assumptions imply a geotherm with a surface heat flow of 80 mW m^{-2}. According to this geotherm, the phengite cooling and resetting temperatures (Ar1 in Fig. 3; Tables 1 and 2) of 360°C correspond to a burial depth of 14 km, which value is taken here as the maximum estimate for the burial depth of the

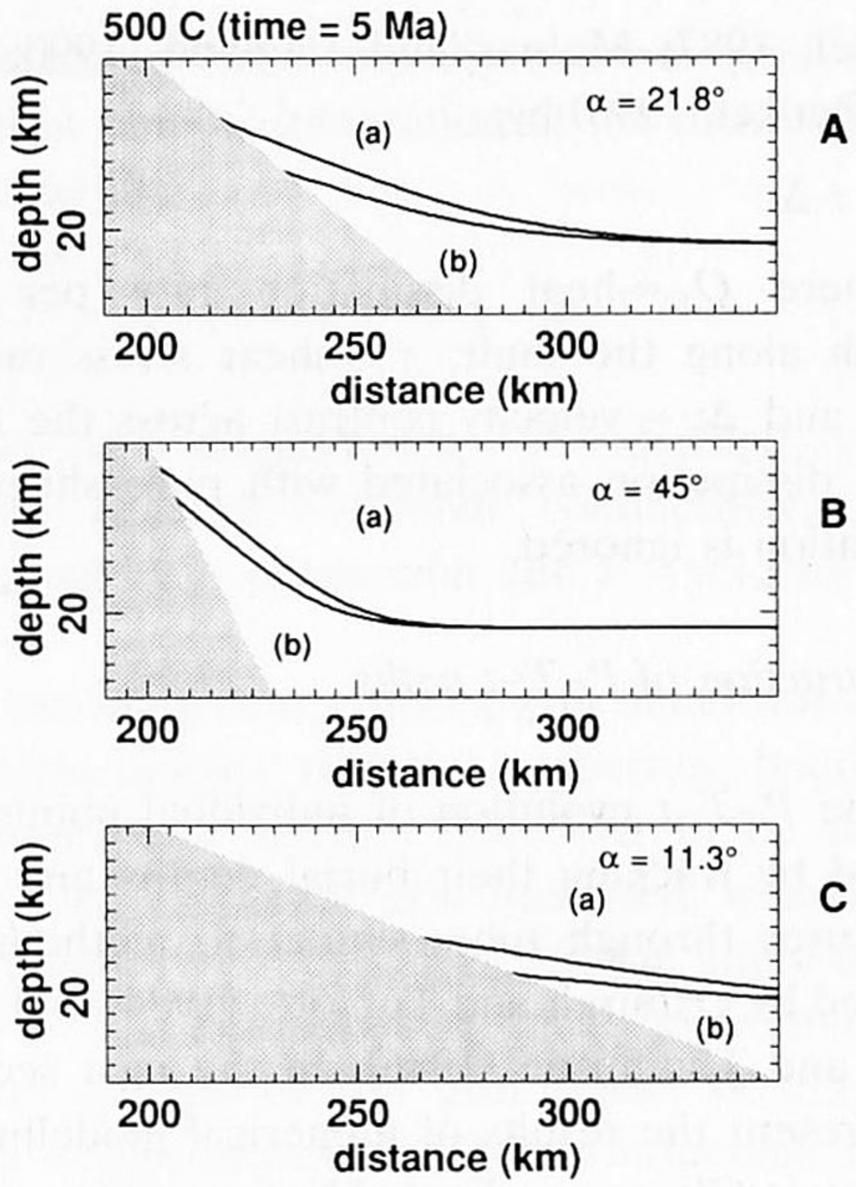

Fig. 7. Heating effect in the hanging wall due to simple shear extension, according to the Wernicke model (Wernicke, 1981). Effects of various amounts of extension and fault angles are depicted. Shaded areas denote the footwall, non shaded areas denote the hanging wall. Extension occurred over a time interval of 5 Ma. The rise of the 500°C isotherm in the hanging wall, due to finite extension, is given. Curve a = 100 km finite extension; curve b = 50 km finite extension. (A) The tangent of the fault angle = 0.4. (B) The tangent of the fault angle = 1.0. (C) The tangent of the fault angle = 0.2.

Mulhacén complex (in the eastern Sierra de Los Filabres) at the onset of extension. The Alpujárride complex experienced a T_{max} of 450°C prior to heating (Bakker et al., 1989; De Jong, 1991). Therefore, the burial depth of the higher Alpujárride nappes prior to extension must occur at crustal levels, where temperatures do not exceed 450°C. According to the initial steady state geotherm, this temperature corresponds to a burial depth of 19 km.

Modes of lithospheric extension

Wernicke simple shear: In our first model to account for the heating observed, the Wernicke simple shear mechanism (Wernicke, 1981; Voorhoeve and Houseman, 1988) is adopted. We took a period of 5 Ma for the duration of extension. We examined the heating effect at the hanging wall for various amounts of finite extension and various fault angles (Fig. 7). To satisfy the thermal constraints of heating in the Wernicke simple shear models in Figure 7, we represent the Mulhacén complex and the higher Alpujárride nappes by a 75 km long line segment in the hanging wall, parallel to the 500°C isotherm, which corresponds to the thermal situation at the end of extension. This line segment must fulfil the constraints on burial depths for the Mulhacén complex (14 km) and the Alpujárride complex (less than 19 km). The modelling demonstrates that only very low-angle faults (Fig. 7C) can explain the observed widespread heating. Figure 7C also shows that, for the rather high value of 100 km for the finite extension, heating to 500°C is predicted within the depth range specified. In this case, we assume that the Mulhacén complex is located close to the fault at depths approaching 14 km, whereas the higher Alpujárride nappes are located further to the right (east) at greater depths. The Wernicke model, however, fails to explain temperatures exceeding 500°C and, therefore, does not provide a plausible mechanism for the widespread heating in the Betic Zone. Furthermore, the predicted homogenous upwarp of subcrustal isotherms in the footwall block is not consistent with the observed concentrated occurrence of ultramafic rocks associated with Alpujárride nappes in the westernmost Betics.

Delaminated simple shear: In our second approach to explain heating by a simple shear model, the delamination mechanism (Lister et al., 1986) is used. In this model, the simple shear fault is marked by a "staircase" geometry (Fig. 8). This geometry reflects contrasting rheological properties within the lithosphere. Starting from the surface, the fault cuts down the brittle upper crust at a high angle, deviates to a low angle in the ductile lower crust (Melosh, 1990) and bends back again to a high angle in the brittle subcrustal lithosphere. Fault motion is modelled assuming simple shear kinematics (eqn. (3), Fig. 5). The results given in Figure 8 show that, in contrast to the Wernicke model, the delamination model can explain widespread heating to 500°C in a narrow range of burial depths and with a moderate finite extension. For models in which the fault penetrates in the subcrustal lithosphere at high angles

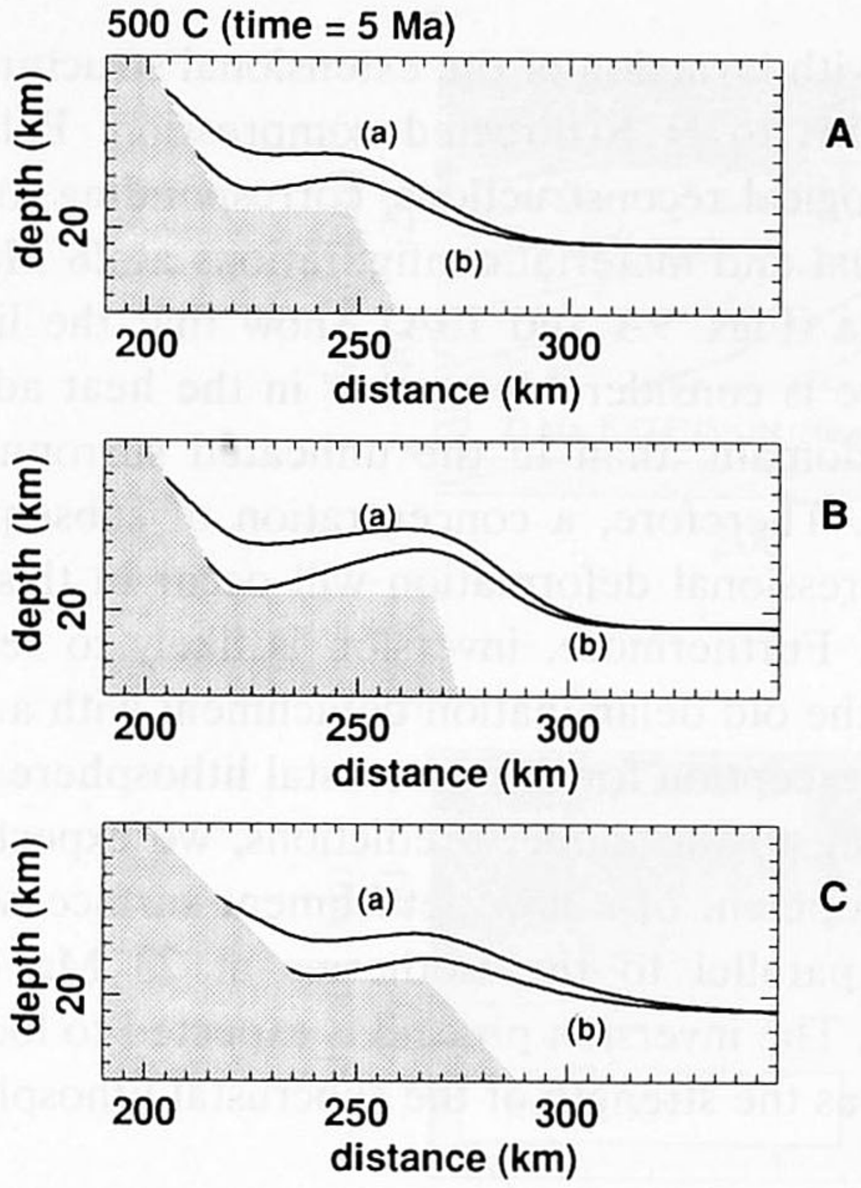

Fig. 8. Heating effect in the hanging wall due to simple shear extension, according to the delamination model (Lister et al., 1986). The horizontal extension of the fault corresponds to ductile behaviour in the lower crust (Melosh, 1990). Footwall deformation is characterised by simple shear kinematics only (Fig. 5). Effects of various amounts of extension and different fault geometries are depicted. Shaded areas denote the footwall, non shaded areas denote the hanging wall. Extension takes place in a time interval of 5 Ma. The rise of the 500°C isotherm in the hanging wall, due to finite extension, is given. Curve (a) = 100 km finite extension, curve (b) = 50 km finite extension. (A), (B) and (C) depict heating effects for different fault geometries.

with a large horizontal extent of the fault in the lower crust (Fig. 8b), pronounced upwarp of subcrustal temperatures occurs in the zone of the steeply dipping fault. This feature is consistent with the observed concentrated occurrence of ultramafic rocks associated with Alpujárride nappes in the westernmost Betics. Therefore, it seems that the delamination extension model consistently explains the main characteristics of the heating of the Mulhacén complex and higher Alpujárride nappes.

Combined shear: The "staircase" delaminated shear model is characterised by concentrated vertical advection of heat in the region where the fault cuts at steep angle through the subcrustal lithosphere. Translation along the low-angle parts of the fault results in the lateral distribution of heat. The thermal consequences of this model are in many respects very similar to a combined shear model (Figs. 5 and 6), in which the steeper part of the fault in the subcrustal lithosphere is substituted by a narrow zone of pure shear deformation.

Role of intrusives: Thermal perturbations by intrusives can locally contribute to reheating and therefore amplify the large scale heat advection, induced by lithospheric extension. The regional scale of the observed reheating pattern, however, rules out a dominant control by localised intrusives. This is confirmed by the observed long wavelength patterns of gravity anomalies (Casas and Carbó, 1990).

Effects of shear heating and fluid transport: We have investigated for both the Wernicke and delamination models effects of frictional and dissipative heating and fluid migration. For frictional and dissipative heating we adopted a value of 1 km for the width of the fault zone in the ductile domains. Calculations incorporating these effects resulted in an increase in temperature of less then 10°C. Therefore, we have ignored the effects of frictional and dissipative heating. Furthermore, dehydration accompanying a greenschist to amphibolite facies change results in liberation of 3% mass percent H_2O (Fyfe, 1985). Assuming a rock pile of 5 km undergoing this facies change, the resulting fluid migration involves a rise of temperature in the order of 10°C, suggesting that fluid migration also has a minor effect on total heating. We, therefore, ignored the heating effects of friction and dissipation and fluid migration.

Mode of lithospheric extension in the Betics: The thermal modelling demonstrates that the *P–T–t* evolution in the eastern Betics can adequately be explained by a model involving delaminated simple shear. Below we will explore the consequences of this model for the thermo-mechanical evolution of the area.

Thermo-mechanical models for lithospheric extension and compression

Extension: Results given in Figures 9A and 10A, show the pre-extensional (28 Ma) and post-

extensional (23 Ma) configurations respectively for the delaminated shear model. During extension, exhumation of the Mulhacén complex with uplift of the order of 3 km (Fig. 3) occurred, and this feature is incorporated in our model. Precise estimates for the magnitude of the exhumation of the higher Alpujárride nappes during extension are lacking, but the uplift is probably of the same order of magnitude. The exhumation and associated cooling effects were ignored in the previous analyses, because of their modest influence on the advective heating. The resulting P–T–t evolutions for various parts of the complexes show that a finite extension of 80 km is sufficient to explain widespread heating.

Inversion: After heating the Mulhacén complex experienced rapid cooling, which is consistent with inversion of the extensional structure by NW–SE to N–S directed compression. Palaeorheological reconstructions, corresponding to the thermal and material configurations at 28 Ma an 23 Ma (Figs. 9A and 10A), show that the lithosphere is considerably weaker in the heat advection domain, than in the unheated surrounding areas. Therefore, a concentration of subsequent compressional deformation will occur in this domain. Furthermore, inversion is likely to reactivate the old delamination detachment with a possible exception for the subcrustal lithosphere. According to the model predictions, we expect the development of a new detachment surface which dips parallel to the isotherms at 23 Ma (Fig. 10A). The inversion process is expected to lock as soon as the strength of the subcrustal lithosphere,

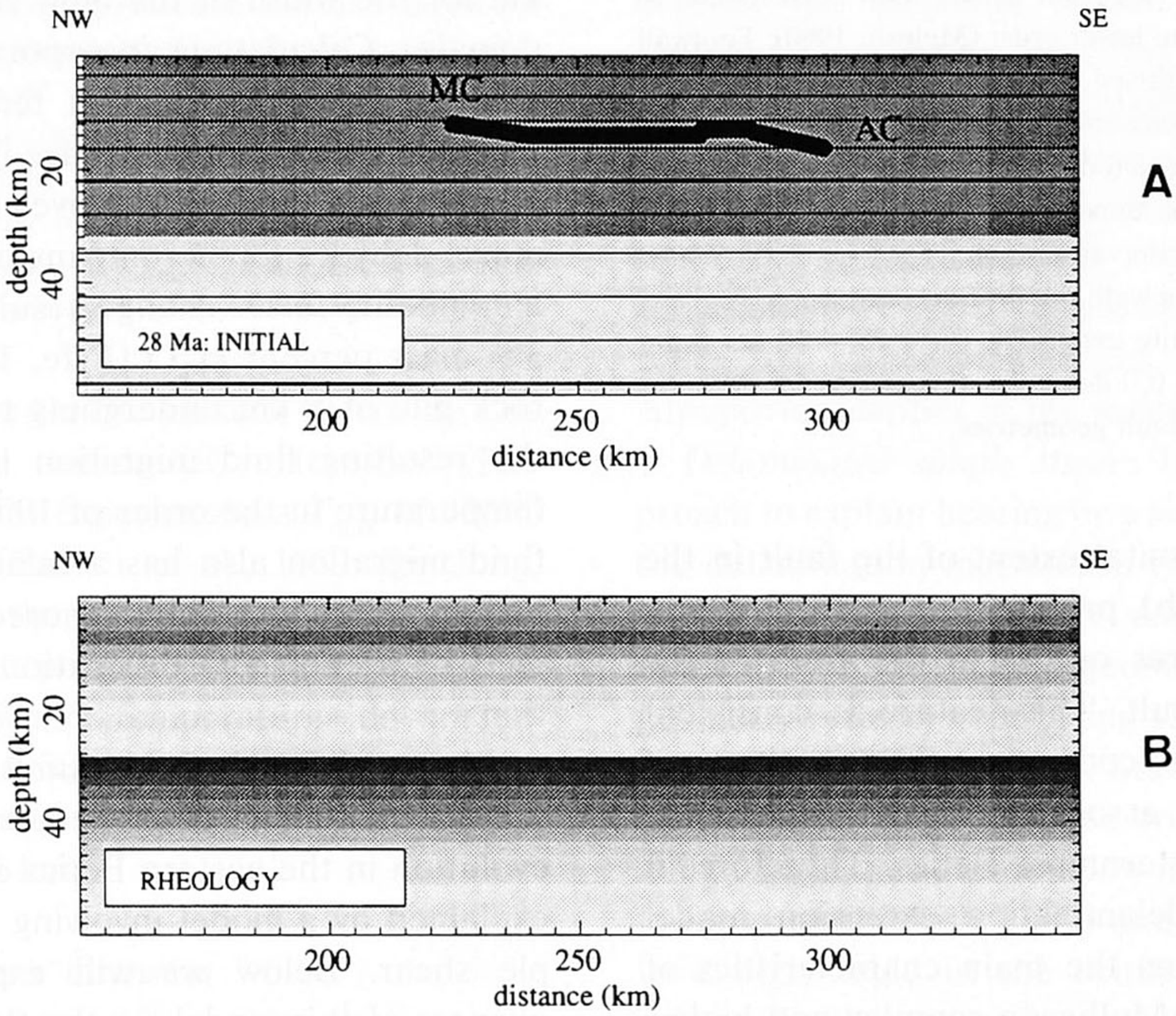

Fig. 9. Thermo-tectonic and rheological configurations in latest Oligocene times (28 Ma) in the eastern Betics. (A) Thermo-tectonic configuration. Dark shaded areas depict crustal material, light shaded areas mantle material. Thermal distributions are contoured in 100°C intervals. The Mulhacén complex (*MC*) and the higher Alpujárride nappes (*AC*) are depicted by black bars. See text for discussion. (B) Paleo-rheological reconstructions, corresponding to the thermal configuration (Fig. 9A). Rheological parameters for crust and mantle rocks are based on extrapolation from rock mechanics data (Carter and Tsenn, 1987) and are listed in Table 3. A strain rate of 10^{-12} was adopted (Van den Beukel, 1990) and compressional deformation is assumed. Areas of dark shading exhibit higher strength than areas of lighter shading. Grey scale is linear, ranging from zero to a maximum of 1600 MPa. See text for discussion.

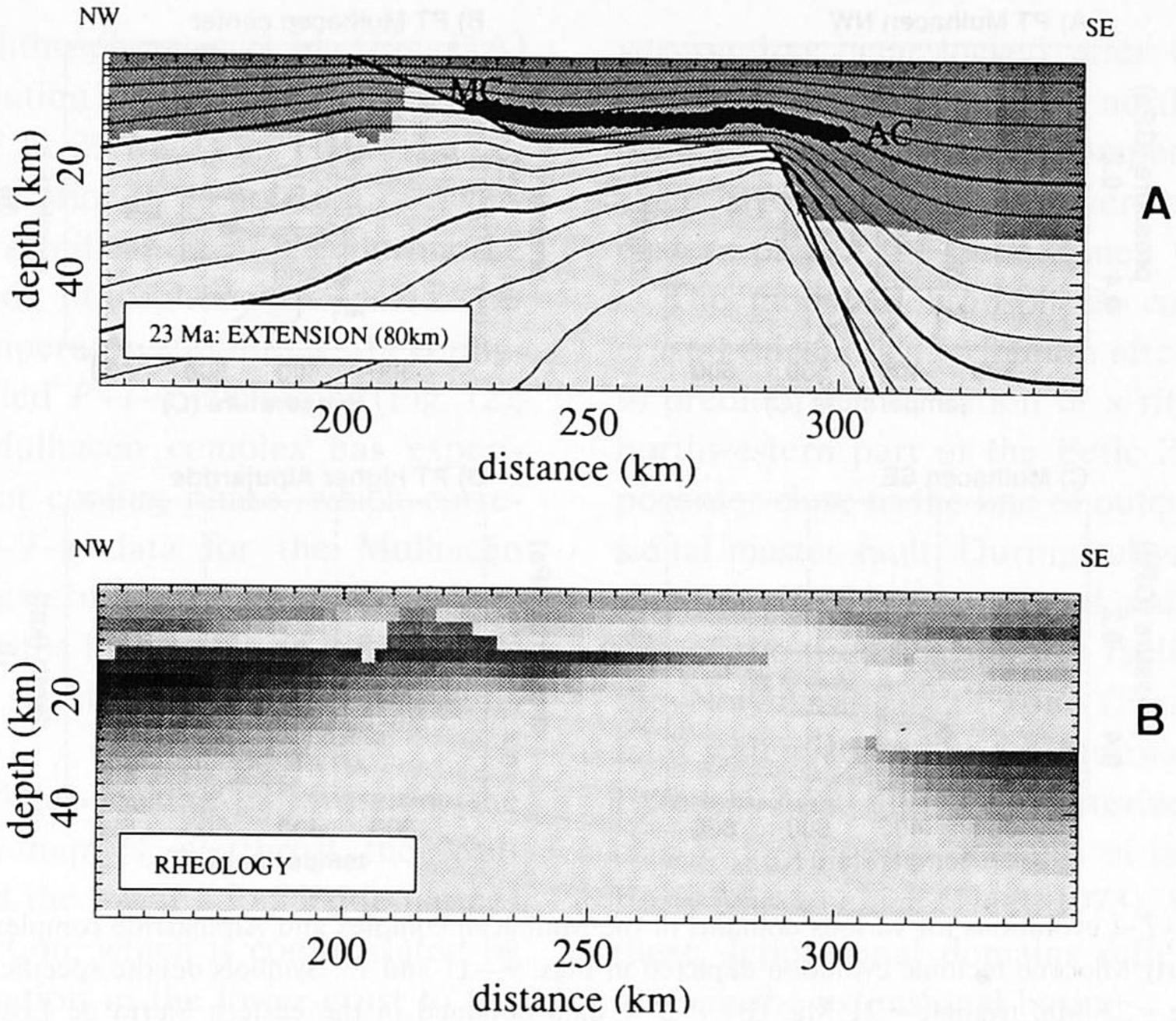

Fig. 10. Thermo-tectonic and rheological configurations in latest Oligocene times (23 Ma) in the eastern Betics. See Fig. 9A and 9B for explanation.

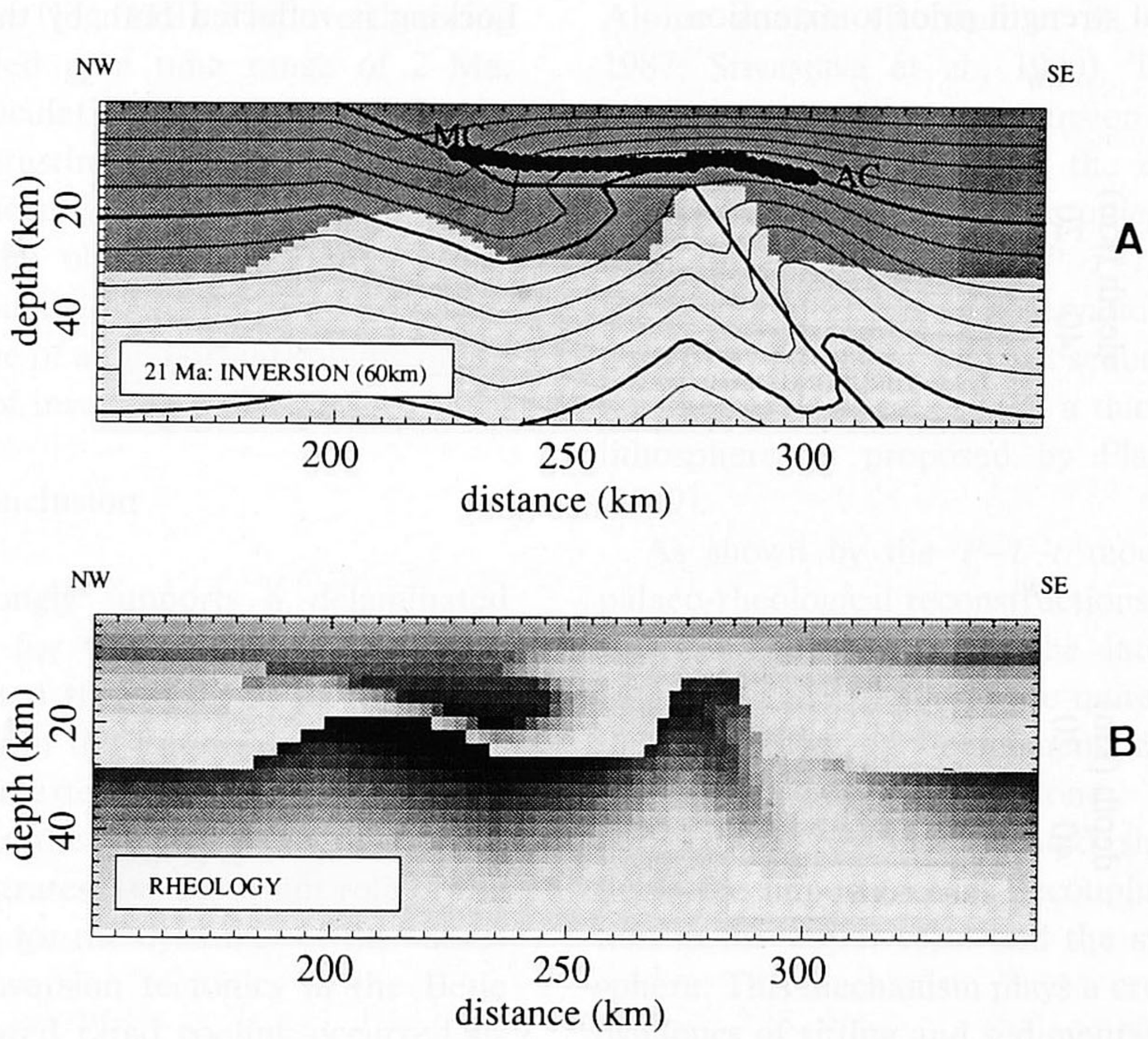

Fig. 11. Thermo-tectonic and rheological configurations in Early Miocene times (21 Ma) in the eastern Betics. Figure conventions as in Fig. 9.

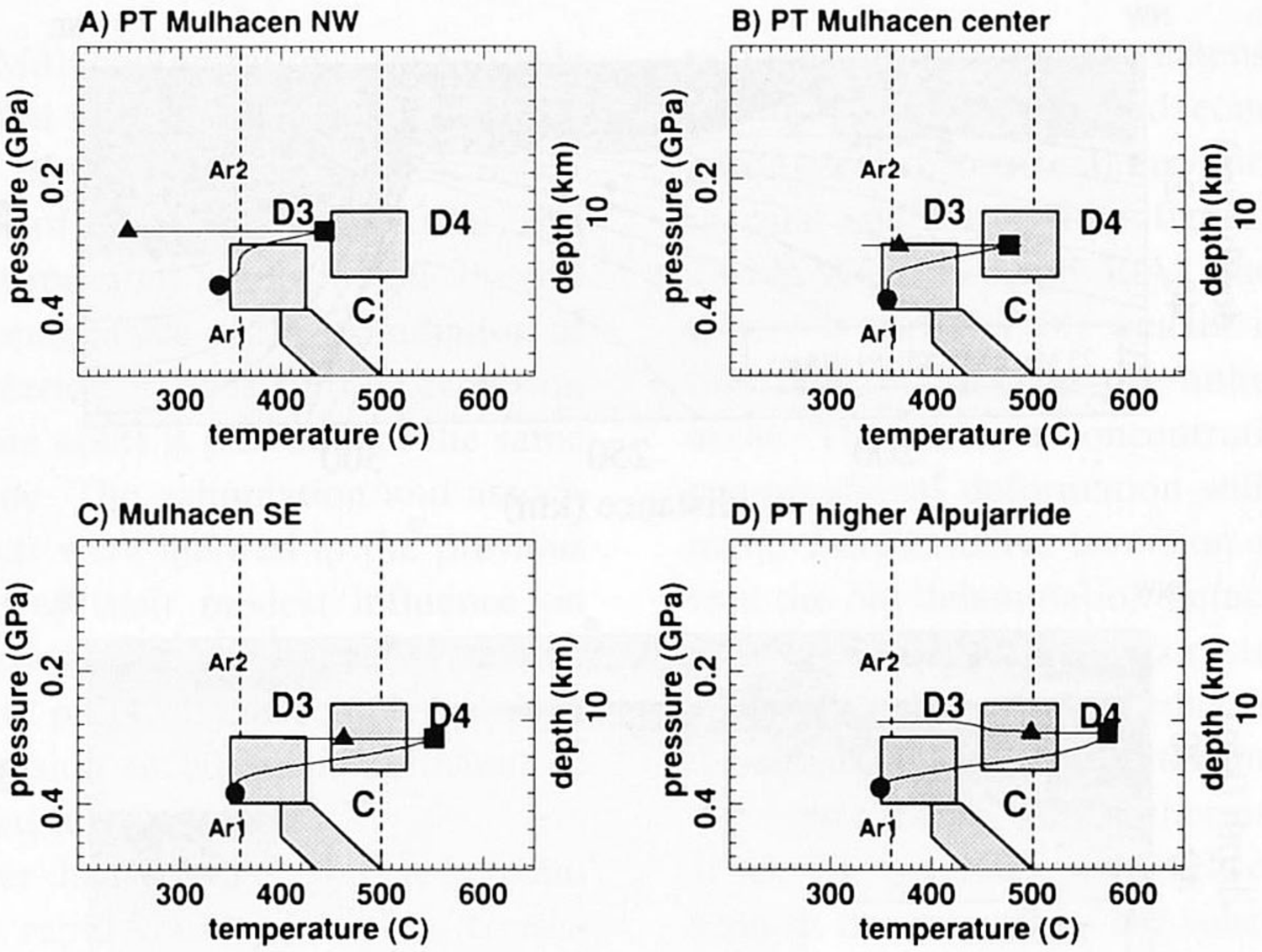

Fig. 12. Modelled P–T–t evolutions for various domains in the Mulhacén complex and Alpujárride complex, corresponding to the latest Oligocene–Early Miocene tectonic evolution depicted in Figs. 9—11 and 13. Symbols denote specific ages during evolution: dot = 28 Ma, square = 23 Ma, triangle = 21 Ma. (B) P–T–t data obtained in the eastern Sierra de Los Filabres. See text for discussion.

which determines the main part of the strength of the lithosphere, has reached values corresponding to its original strength prior to extension.

According to the model calculations (Fig. 11), inversion locks after 60 km of finite convergence. Locking is reflected both by the strength values

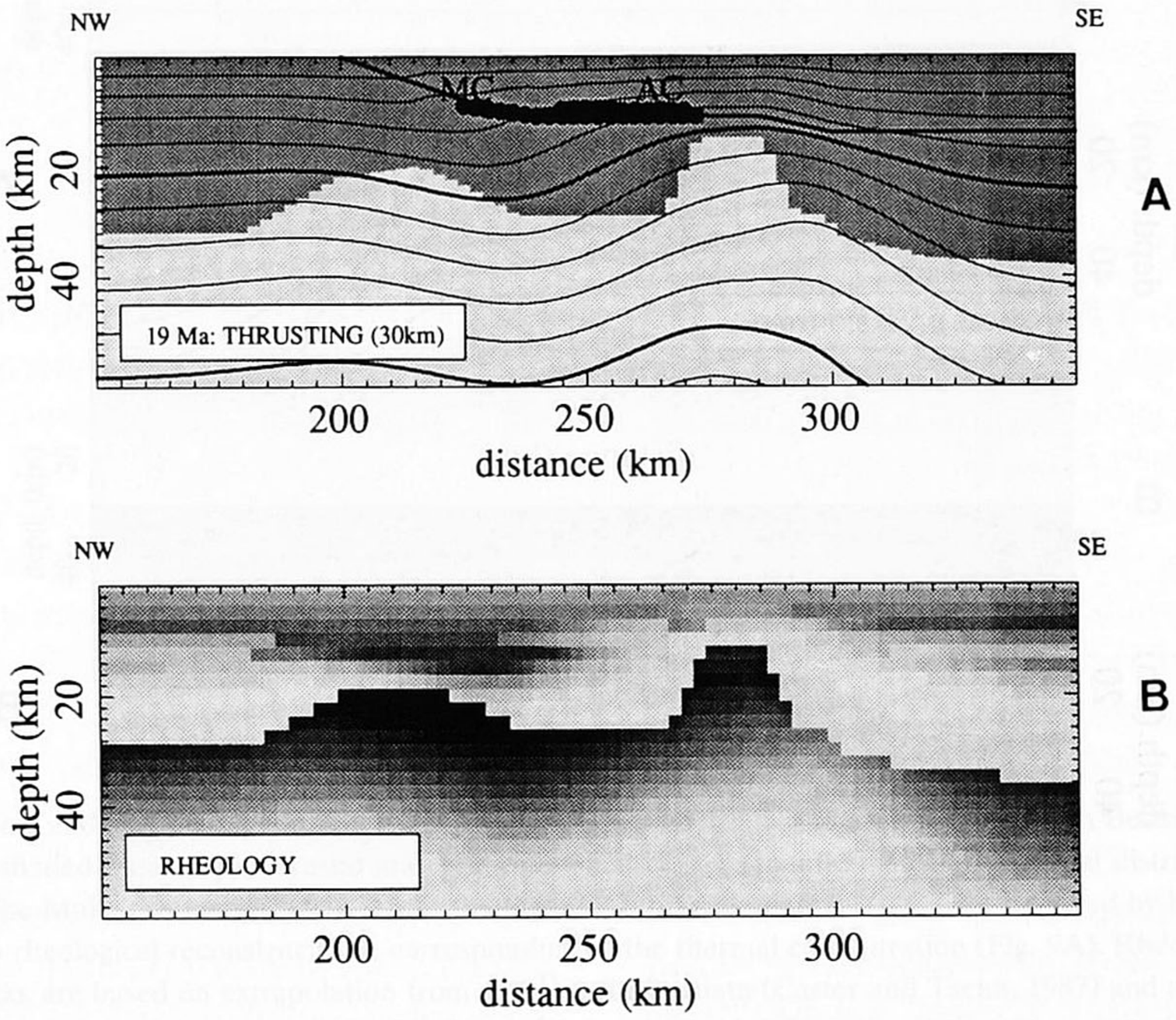

Fig. 13. Thermo-tectonic and rheological configurations in the Early Miocene (19 Ma) in the eastern Betics. See Fig. 9A and 9B for explanation. See text for discussion.

for the subcrustal lithosphere at 21 Ma (Fig. 11A) and by the distribution of isotherms in the subcrustal lithosphere at 21 Ma (Fig. 11B). The occurrence of locking prior to completion of inversion, follows from significant heat loss during the preceding phase of lithospheric extension. Inspection of the temperatures in the 21 Ma configuration and modelled *P–T–t* evolutions (Fig. 12), shows that the Mulhacén complex has experienced an important cooling phase, which corresponds to the *P–T–t* data for the Mulhacén complex in the eastern Sierra de Los Filabres (Fig. 12B), whereas the higher Alpujárride nappes have experienced significantly less cooling (Fig. 12D).

Overthrusting: After locking of inversion, the upper Alpujárride nappes overthrust the Mulhacén complex and the lower Alpujárride nappes in northward direction, which is compensated by pure shear deformation in the lower crust to the southeast. The overthrusting and pure shear deformation is concentrated in zones of pronounced lithospheric weakness, predicted by the palaeo-rheological reconstruction at the completion of the inversion phase (Fig. 11B). The overthrusting process is modelled in a time range of 2 Ma. Results of the calculations are shown in Figure 13. During overthrusting, the higher Alpujárride nappes are significantly cooled. Both the model predictions and the observed *P–T–t* evolution for the higher Alpujárride nappes (Fig. 12D) support the occurrence of an important cooling phase after the locking of inversion at 21 Ma.

Discussion and conclusion

Our study strongly supports a delaminated shear mechanism for the extensional processes that have dominated the latest Oligocene–Early Miocene evolution in the Betic Zone. It appears that 80 km of finite extension can account for the observed heating in the eastern Betics. The modelling also demonstrates the important role of the mode of extension for the dynamics of the subsequent phase of inversion tectonics in the Betic Zone. The associated rapid cooling occurred simultaneously with a phase of inversion tectonics. The palaeo-rheological profiles suggest that inversion has been locked after 60 km of finite convergence. Subsequent northward directed overthrusting has been compensated by pure shear deformation of the lower crust in the southeastern part of the Betic Zone.

The modelled lithospheric configuration and crustal thickness distribution after extension (Fig. 9) predicts the formation of a rifted basin in the northwestern part of the Betic Zone, with a depocenter close to the line of outcrop of the extensional master fault. During subsequent compression this rifted basin is closed and overthrust. The site of the predicted master fault corresponds to the North Betic fault zone (Fig. 2). This major fault system separates the Internal Zone from the External Zone and is characterized by telescoped clastic depositional domains of latest Oligocene–Early Miocene age (Geel, 1973). We propose that these depositional domains reflect distinct positions in the extensional basin.

The latest Oligocene–Early Miocene extension in the Betic Zone is associated with stress patterns in the Eurasian plate and initiation of extensional features in the overall convergent Alpine domain (Rehault et al., 1984; Bergerat, 1987; Srivastava et al., 1990). The lithospheric configuration prior to extension reflects conditions of elevated heat and the extension phase followed a stage of tectonic quiescence, as indicated by the established *P–T–t* paths (Fig. 3, Tables 1 and 2). These observations strongly suggest that extension and subsequent heating are not the result of collapse of a thickened and cold lithosphere as proposed by Platt and Vissers (1989).

As shown by the *P–T–t* modelling and the palaeo-rheological reconstructions, the conditions of elevated heat during the latest Oligocene–Early Miocene evolution are quite favourable for the formation of detachment zones at lower crustal levels in the Betic Zone.

The proposed delaminated shear model reflects the importance of decoupling of deformation in the upper crust and the subcrustal lithosphere. This mechanism plays a crucial role in the dynamics of rifting and sedimentary basin formation (see also Reston, 1990). This model is also supported by observations of elevated heat flow

and shoulder uplift in a large number of rifted basins (Buck et al., 1988; Ziegler, 1990), reflecting the predicted existence of a narrow zone of subcrustal extension beneath a different and more homogenous extending upper crust (Kooi et al., 1991).

As pointed out by many authors (Vegas and Banda, 1982; De Jong, 1990; Van der Beek and Cloetingh, 1992-this volume), the Betic Zone has undergone a long polyphase history of repeated extension and compression following a prolonged stage of Mesozoic rifted basin evolution of the extensional Betic margin (Peper and Cloetingh, 1992-this volume). The thermo-mechanical modelling of the Betics presented in this paper provides new quantitative insights into the complex evolution of the westernmost Mediterranean area, in particular of the Valencia trough and Alboran basin, and contributes to a better understanding of the dynamics of extension and compression in the lithosphere in general.

Acknowledgements

We thank Cees Biermann, Henk Helmers and Fred Beekman for useful discussions and suggestions, and two anonymous reviewers for constructive comments. This research is funded by a grant from the Earth Science Branch (AWON) of the Netherlands Organisation for Research (NWO).

References

Albert-Bertrán, J.F., 1979. Heat flow and temperature gradient data from Spain. In: V. Cermak and L. Rybach (Editors), Terrestrial Heat Flow in Europe. Springer, Berlin, pp. 261–266.

Bakker, H.E., de Jong, K., Helmers, H. and Biermann, C., 1989. The geodynamic evolution of the Interal Zone of the Betic Cordillèras (south-east Spain): a model based on structural analysis and geothermobarometry. J. Metamorphic Geol., 7: 359–381.

Banda, E., 1988. Crustal parameters in the Iberian Peninsula. Phys. Earth Planet. Inter., 51: 222–225.

Banda, E. and Ansorge, J., 1980. Crustal structure under the central and eastern part of the Betic Cordillera. Geophys. J.R. Astron. Soc., 63: 515–532.

Banda, E., Ansorge, J., Boloix, M. and Cordoba, D., 1980. Structure of the crust and upper mantle beneath the Balearic Islands (Western Mediterranean). Earth Planet. Sci. Lett., 49: 219–230.

Banda, E., Udias, A., Mueller, St., Mezcua, J., Boloix, M., Gallart, J. and Aparicio, M., 1983. Crustal structure beneath Spain from deep seismic sounding experiments, Phys. Earth Planet. Inter., 31: 277–280.

Barranco, L.M., Ansorge, A. and Banda, E., 1990. Seismic refraction constraints on the geometry of the Ronda peridotite massif (Betic Cordillera, Spain). Tectonophysics, 184: 379–392.

Behrman, J. and Platt, J.P., 1982. Sense of nappe emplacement inferred from quartz c-axis fabrics: an example from the Betic Cordilleras (Spain). Earth Planet. Sci. Lett., 59: 208–215.

Bellon, H. and Brousse, R., 1977. Le magmatisme périméditerranéen occidental. Essai de synthèse. Bull. Soc. Géol Fr., 7: 469–480.

Bergerat, F., 1987. Stress fields in the European Platform at the time of Africa–Eurasia collision. Tectonics, 6: 99–132.

Buck, W.R., Martínez, F., Steckler, M.S. and Cochran, J.R., 1988. Thermal consequences of lithospheric extension: Pure and simple. Tectonics, 7: 213–234.

Carter, N. and Tsenn, M., 1987. Flow properties of continental lithosphere. Tectonophysics, 136: 27–63.

Chapman, D.S., 1986. Thermal gradient in the continental crust. In: J.B. Dawson, D.A. Carswell, J. Hall and K.H. Wedepohl (Editors), The Nature of Lower Continental Crust. Geol. Soc. London Spec. Publ., 24: 63–70.

Casas, A. and Carbó, A., 1990. Deep structure of the Betic Cordillera derived from the interpretation of a complete Bouguer anomaly map. J. Geodynam., 12: 137–147.

De Jong, K., 1990. Alpine tectonics and rotation pole evolution of Iberia. Tectonophysics, 184: 279–296.

De Jong, K., 1991. Tectono-metamorphic studies and radiometric dating in the Betic Cordilleras (SE Spain)—with implications for the dynamics of extension and compression in the Western Mediterranean Area. Thesis Vrije Univ. Amsterdam, 204 pp.

De Jong, K., Wijbrans, J.R. and Feraud, G., 1992. Repeated thermal resetting of phengites in the Mulhacén Complex during Miocene extension Betic Zone (SE Spain) shown by $^{40}Ar/^{39}Ar$ step-heating and single grain laser probe dating. Earth Planet Sci. Lett., (submitted).

Duran-Delga, M., 1968. Coup d'oeil sur les unités malaguides des Cordillères Bétiques (Espagne). C.R. Acad. Sci. Paris, 266: 190–193.

Egeler, C.G. and Simon, O.J. 1969. Sur la tectonique de la Zone Bétique (Cordillères Bétiques, Espagne), Verh. K. Ned. Akad. Wet., 25: 90 pp.

England, P.C. and Thompson, A.B., 1986. Pressure–temperature–time paths of regional metamorphism I. Heat transfer during the evolution of regions of thickened continental crust. J. Petrol., 25: 894–928.

Ferrara, G., Bigazzi, G., Bonadonna, F.P. and Giuliani, O., 1973. Radiometric dating of the Valencia volcanic rocks. In: W.B.F. Ryan et al. (Editors), Initial reports of the

Deep Sea Drilling Project, Washington DC, US Govern. Print. Off., 13: 773.

Fonboté, J.M., Guimerà, J., Roca, E., Sàbat, F., Santanach, P. and Fernández-Ortigosa, F., 1990. The Cenozoic geodynamic evolution of the Valencia trough (western Mediterranean). Rev. Soc. Geol. España, 3: 249–259.

Fyfe, W.S., 1985. Global tectonics and resources. Comun. Serv. Geol. Port., 71: 3–15.

Galdeano, A. and Rossignol, J.-C., 1977. Assemblage d'altitude constante des cartes d'anomalies magnétiques couvrant l'ensemble du bassin occidental de la Méditerranée. Bull. Soc. Géol. Fr., 7: 461–468.

Geel, T., 1973. The geology of the Betic of Malaga, the Subbetic, and the zone between these two units in the Velez Rubio area (southern Spain). GUA Pap. Geol., 1 (5): 1–179.

Gómez-Pugnaire, M.T. and Fernández-Soler, J.F., 1987. High pressure metamorphism in metabasites from the Betic Cordilleras (S.E. Spain) and its evolution during the Alpine orogeny. Contrib. Mineral. Petrol., 95: 231–244.

Kooi, H., Burrus, J. and Cloetingh, S., 1991. Lithospheric necking and regional isostasy at extensional basins: part 1, subsidence and gravity modeling with an application to the Gulf of Lions margin (SE France). J. Geophys. Res., submitted.

Kornprobst, J., 1969. Le massif ultrabasique des Beni Bouchera (Rif Interne, Maroc): Etude des Péridotites de haute température et haute pression, et des pyroxenolites á grenat ou sans grenat, qui leur sont associées. Contrib. Mineral. Petrol., 23: 607–618.

Kusznir, N.J., Karner, G.D. and Egan, S., 1987. Geometric, thermal and isostatic consequences of detachments in continental lithosphere extension and basin formation. In: C. Beaumont and A.J. Tankard (Editors), Sedimentary Basins and Basin-Forming Mechanisms. Can. Soc. Petrol. Geol. Mem., 12: 185–203.

Lister, G.S., Etheridge, M.A. and Symonds, P.A., 1986. Detachment faulting and the evolution of passive continental margins. Geology, 14: 246–250.

Loomis, T.P., 1975. Tertiary mantle diapirism, orogeny and plate tectonics east of the Strait of Gibraltar. Am. J. Sci., 275: 1–30.

Lundeen, M.T., 1978. Emplacement of the Ronda peridotite. Sierra Bermeja, Spain. Geol. Soc. Am. Bull., 89: 172–180.

Maillard, A., Brunet, M.F., Desegaulx, P., Foucher, J.P., Mauffret, A. and Steckler, M., 1990. Geothermal model of the formation of the Valencia Trough. Terra Abstracts, 2: 114.

Martí, J., Grachev, A., Mitjavila, J., Aparicio, A. and Roca, E., 1990. Cenozoic magmatism in the Valencia Trough. Terra Abstracts, 2: 114.

Melosh, H.J., 1990. Mechanical basis for low-angle normal faulting in the Basin and Range Province. Nature, 343: 331–335.

Molnar, P. and England, P., 1990. Temperature, heat flux, and frictional stress near major thrust faults. J. Geophys. Res., 95: 4833–4856.

Monié, P., Galindo-Zaldivar, J., Gonzalez Lodeiro, F., Goffé, B. and Jabaloy, A., 1991. $^{40}Ar/^{39}Ar$ geochronology of Alpine tectonism in the Betic Cordilleras (southern Spain). J. Geol. Soc. London, 148: 289–297.

Oxburgh, E.R. and Turcotte, D.L., 1974. Thermal gradients and regional metamorphism in overthrust terrains with special reference to the eastern Alps. Schweiz. Mineral. Petrogr. Mitt., 54: 641–662.

Platt, J.P. and Vissers, R.L.M., 1989. Extensional collapse of thickened continental lithosphere: A working hypothesis for the Alboran Sea and Gibraltar arc. Geology, 17: 540–543.

Peper, T. and Cloetingh, S., 1992. Lithospheric dynamics and the tectono-stratigraphic evolution of the Mesozoic Betic rifted margin (SE Spain). In: E. Banda and P. Santanach (Editors), Geology and Geophysics of the Valencia Trough, Western Mediterranean. Tectonophysics, 203: 345–361.

Pollack, H.N. and Chapman, D.S., 1977. On the regional variation of heat flow, geotherms and lithospheric thickness. Tectonophysics, 38: 279–296.

Priem, H.N.A., Boelrijk, N.A.I.M., Hebeda, E.H., Oen, I.S. Verdurmen, E.A.Th and Verschure, R.H., 1979. Isotopic dating of the emplacement of the ultramafic masses in the Serrania de Ronda, southern Spain. Contrib. Mineral. Petrol., 70: 103–109.

Purdy, J.W. and Jäger, E. 1976. K-Ar ages on rock forming minerals from the Central Alps. Mem. Ist. Geol. Mineral. Univ. Padova, 30: 1–31.

Rehault, J.P., Boillot, G. and Mauffret, A., 1984. The western Mediterranean basin geological evolution. Mar. Geol., 55: 447–477.

Reston, T.J., 1990. Shear in the lower crust during extension: not so pure and simple. Tectonophysics, 173: 175–183.

Ricou, L.E., Dercourt, J., Geysant, J., Grandjaquet, C., Lepvrier, C. and Biju-Duval, B., 1986. Geological constraints on the Alpine evolution of the Mediterranean Tethys. Tectonophysics, 123: 83–122.

Simon, O.J., 1987. On the Triassic of the Betic Cordilleras (Southern Spain). Cuad. Geol. Iber., 11: 385–402.

Simon, O.J., Westerhof, A. and Rondeel, H.E., 1976. A propos d'une nouvelle paléogéographie de la zone Bétique (Espagne méridionale): Implication geodynamique Bull. Soc. Géol. Fr., 3 (18): 603–615.

Srivastava, S.P., Roest, W.R., Kovacs, L.C., Oakey, G., Lévesque, S., Verhoef, J. and Macnab, R., 1990. Motion of Iberia since the Late Jurassic: Results from detailed aeromagnetic measurements in the Newfoundland Basin. Tectonophysics, 184: 229–260.

Stephenson, R., 1989. Beyond first-order thermal subsidence models for sedimentary basins? In: T.A. Cross (Editor), Quantitative Dynamic Stratigraphy. Prentice Hall, Englewood Cliffs, NJ, pp. 113–125.

Torres-Roldán, R.L., 1981. Plurifacial metamorphic evolution

of the Sierra Bermeja peridotite aureole (southern Spain). Est. Geol., 37:115–133.

Tubía., J.M. and Cuevas, J., 1986. High-temperature emplacement of the Los Reales peridotite nappe (Betic Cordillera, Spain). J. Struc. Geol., 8: 473–482.

Van den Beukel, J., 1990. Thermal and mechanical modelling of convergent plate margins. Geol. Ultraiectina, 62: 1–126.

Van den Beukel, J. and Wortel, R., 1987. Temperatures and shear stresses in the upper part of a subduction zone. Geophys. Res. Lett., 14: 1057–1060.

Van den Bosch, J.W.H., 1974. Quelques principes généraux de l'interprétation gravimetrique illustrés par des exemples empruntés de la carte gravimétrique du Maroc (structure du Rif et intrusions granitiques au Maroc central). Notes Serv. Geol. Maroc, 35: 117–136.

Van der Beek, P.A. and Cloetingh, S., 1992. Lithospheric flexure and the tectonic evolution of the Betic Cordilleras (SE Spain). In: E. Banda and P. Santanach (Editors), Geology and Geophysics of the Valencia Trough, Western Mediterranean. Tectonophysics, 203: 325–344.

Vegas, R. and Banda, E., 1982. Tectonic framework and Alpine evolution of the Iberian Peninsula. Earth Evolution Sci., 4: 320–343.

Verwer, J.G., 1977. A class of stabilized three-step Runge Kutta methods for the numerical integration of parabolic equations. J. Comp. Appl. Math., 3: 155–166.

Voorhoeve, H. and Houseman, G., 1988. The thermal structure of lithosphere on a low-angle detachment zone. Basin Res., 1: 1–9.

Völk, H.R. and Rondeel, H.E., 1967. Zur Gliederung des Jungtertiars im Becken von Vera, Sudost Spanien. Geol. Mijnbouw, 43: 310–315.

Wernicke, B., 1981. Low-angle normal faults in the Basin and Range Province-nappe tectonics in an extending orogen, Nature, 291: 645–648.

Westerhof, A.B., 1977. On the contact relations of high temperature peridotites in the Serrania de Ronda, southern Spain. Tectonophysics, 39: 579–592.

Zeyen H.J., Banda, E., Gallart, J. and Ansorge., J., 1985. A wide angle seismic reconnaissance survey of the crust and upper mantle in the Celtiberian Chain of eastern Spain. Earth Planet. Sci. Lett., 75: 393–402.

Ziegler, P.A., 1990. Geological Atlas of Western and Central Europe—second and completely revised edition. Geological Society Publishing House, Avon (UK): 239pp.